Simulation of correlated and uncorrelated packing of random size spheres

A. Yang, C. T. Miller, and L. D. Turcoliver
Department of Environmental Sciences and Engineering, 114 Rosenau Hall CB7400, University of North Carolina, Chapel Hill, North Carolina 27599-7400
(Received 7 August 1995; revised manuscript received 10 November 1995)

We present an algorithm to simulate the packing of large samples of spheres chosen from a truncated log-normal distribution for either correlated or uncorrelated distributions. Use of a concept known as the porosity index provides a means to control the final porosity of a packed sample within a range that spans limits approaching random close packing and random loose packing structures. Agreement with previous theoretical, computational, and experimental results is good, and results of previously uninvestigated correlated systems are presented.

PACS number(s): 05.40.+j, 05.45.+b, 81.05.Rm

I. INTRODUCTION

Porous media are significant in applications throughout science and engineering fields; fluid flow and species transport in such systems are frequently of interest. Macroscopic continuum approaches are constructed by averaging over a representative elementary volume of porous media and are often used to derive fundamental mass, momentum, and energy balance laws [1]. However, these approaches require constitutive relations to close the system of equations. Constitutive relations for single and multiple phase fluid flow in porous media are often empirically based (e.g., extended Darcy's law, pressure-saturation-permeability relations) [2–4], but can be approached theoretically as well [5]. Theoretical approaches for deriving such constitutive relations require knowledge of flow and transport phenomena at the pore scale, and approaches to compute the relevant statistical moments of the transport phenomena quantities of interest at the macroscopic scale of concern. This in turn requires an understanding of the pore structure of the porous media, which necessitates either extensive small-scale experimental measurements or a theoretical approach for constructing a meaningful representation of the pore structure. Because of the difficulty, expense, and time required to determine the pore structure experimentally, theoretical approaches are conceptually appealing.

Many porous media systems can be represented in a simplified manner as packed arrangements of spheres. To be realistic, the size, porosity, and coordination number distributions of the spherical packings should be similar to those of the system being simulated. Further, many natural porous media systems are stochastic and are often characterized by correlated random fields in space [6]. It is expected that pore-size morphology distributions caused by nonuniform media, variations in packing arrangement, and spatial correlation will lead to significant variations in certain macroscopic properties of applied interest, such as residual saturation of a nonwetting fluid in a two-fluid multiphase system [7]. To date, published approaches to the packing problem have typically been restricted in the porosity range considered and the size of the system simulated. They have also been limited to either a uniform or purely random spatial correlation structure of the media.

The objectives of this work were: (1) to develop an efficient algorithm capable of simulating a large number of random-size spheres over a broad range of porosities, for both uncorrelated and correlated structures; (2) to compare results from the application of the developed algorithm to existing theoretical, computational, and experimental results for similar systems; and (3) to evaluate the effect of media properties on pore structure characteristics for previously uncharacterized systems.

II. BACKGROUND

Meeting these objectives required a complete description of the pore morphology of a randomly packed porous media typical of natural systems; therefore, approaches relying on either systematic packing or yielding bulk properties alone, such as porosity and coordination number, were not appropriate. These constraints led to the consideration of random packing simulation models. Two types of such models were given primary consideration: sequential addition and collective rearrangement.

Sequential addition packing models start with a small seed cluster of spheres and serially add a single sphere at the surface of the cluster so that the added sphere contacts three existing spheres. Several algorithms have been developed for choosing the position of an added sphere [8–12]. Although sequential addition models have the advantage of simulating relatively large systems of homogeneous spheres, they yield only a relatively loose packing structure (high porosity, ϕ), provide no explicit mechanism to control ϕ, produce final packing distributions that may be radially inhomogeneous [8], and have not been used to produce packings of random spheres with a specified spatial correlation.

Though sequential addition models have significant

drawbacks, two key concepts can be gleaned from their construction: rolling to obtain stable support and position ordering. In sequential addition methods, a new sphere is brought into contact with the surface of the existing sphere pack. The sphere is then rolled along the surface of the original contacting sphere until it is in contact with two additional neighboring spheres, yielding a three-sphere, nonoverlapping support. By repeating the process multiple times for a vertically growing packed structure, ordering the final positions by vertical position, and choosing the lowest position from among the set of trials, Visscher and Bolsterli [9] decreased ϕ from 0.418 to 0.400.

Collective rearrangement is the second major class of spherical packing algorithm, in which packing porosities typical of random, dense-packed systems can be simulated. These algorithms consist of two main steps: initial sphere size generation and placement, and iterative rearrangement to achieve an overlap-free condition. Initial sphere size generation and placement is typically accomplished by simulated sampling from a given probability density function—such as uniform or log normal—and locating all spheres randomly within a given domain, permitting overlaps. Iterative rearrangement is then applied to remove overlaps, a procedure in which different types of relaxation techniques have been used [13–16]. Iterative rearrangement methods, such as compression of a hard-sphere gas, Monte Carlo simulation, and molecular dynamics techniques can generate packings with a porosity and radial distribution similar to experimental results [13,14,17]. However, these methods require intensive computations, which limit potential simulation sizes.

Clarke and Wiley [18] developed an algorithm for the iterative rearrangement of binary mixtures of spheres, which relied upon both the movement along the vector sum of overlapping surrounding spheres and the changing radii of spheres. The packing porosities obtained from this algorithm were similar to the results of uniform ball bearing packings, but only relatively small systems were considered, on the order of 10^3–10^4 spheres. Recently, Nolan and Kavanagh [19,20] presented a repulsive-force algorithm for iterative rearrangement that considered uniform and log-normal distributions of spherical particles. They introduced a particle-bridging mechanism to simulate loose packing and found that the final packing porosity was a function of the initial packing porosity generated before rearrangement. However, due to small simulation sizes, their results showed significant variability.

III. PACKING ALGORITHM

Developing the packing algorithm requires two main procedures: definition of an initial distribution of spherical particles and rearrangement of these spheres to an overlap-free state. Once developed, the algorithm requires definition of (1) an initial domain size, (2) a particle-size density function, (3) an initial correlation structure, (4) an initial porosity (ϕ_0), and (5) a porosity index (I). Alternatively, (4) and (5) can be replaced with a specification of a desired final porosity.

A. Initial particle distribution

The initial distribution of particles is performed for a hexahedral domain with periodic boundary conditions, defined by a length (X), width (Y), and an initial depth (Z). The depth of the domain decreases during the course of the simulation. All boundaries are maintained throughout the simulation using periodic conditions.

Natural solid materials are often described using a log-normal distribution [2,21,22]. Thus, a set of spherical particles is generated by simulated sampling from a probability density function of the form

$$f(\ln r) = \frac{1}{\sqrt{2\pi}\sigma} e^{\frac{-(\ln r - \ln r_o)^2}{2\sigma^2}}, \tag{3.1}$$

where r is the radius of a sphere, σ is the standard deviation in log space of the random variable $\ln r$, and $\ln r_o$ is the mean of the normal distribution. In order to disallow unreasonably large and small values for particle radii, the distribution was clipped to fall within the 99% confidence interval, meaning that the upper and lower 0.5% of the log-normal distribution were truncated. In principle, alternate non-negative probability density functions could be used, but any long-tailed distribution would require truncation, such as that used in the log-normal case.

Samples from the probability density function are used to generate a set of spheres, which are assigned initial, probably overlapping locations within the domain. The initial location of sphere i, denoted as $S_i = S_i(x_i, y_i, z_i)$, for the purely random case is assigned by independent sampling from a uniform distribution, giving $0 \le x_i < X$, $0 \le y_i < Y$, and $0 \le z_i < Z$, where the domain is aligned with and situated at the origin of a Cartesian coordinate system.

For spatially correlated random packing, spheres are located as described above. Radii are assigned based on a mapping of the probability of the nearest neighbor in a spatially-correlated, uniform distribution field (p field) to the corresponding radius in the cumulative probability density function of the spheres. The p field is defined over a regular grid throughout the domain. Gaussian simulation is used to generate the p field using an exponential covariance model of the form [23]

$$C(h_x, h_y, h_z) = \exp\left\{ -\left[\left(\frac{h_x}{l_{cx}}\right)^2 + \left(\frac{h_y}{l_{cy}}\right)^2 + \left(\frac{h_z}{l_{cz}}\right)^2 \right]^{1/2} \right\}, \tag{3.2}$$

where h is the separation distance, and l_c is a correlation length in the respective directions.

Spherical particles are located within the domain and sized using the p-field procedure described above until the initial porosity condition is met:

$$\phi_0 \leq 1 - \frac{4\pi}{3V_t}\sum_{i=1}^{N} r_i^3, \tag{3.3}$$

where ϕ_0 is the initial porosity, V_t is the initial volume of the domain, r_i is the radius of particle i, and N is the total number of particles in the system.

The final step in the initial particle distribution portion of the algorithm is to assign each particle to a cell location within the domain in order to facilitate the location of neighboring spheres needed for rearrangement. Cells are established by dividing the domain into many small cubic volumes of uniform size, each (d_c) slightly larger than the maximum sphere diameter (D_m); i.e., $d_c = D_m + \delta$, where $\delta \ll D_m$. Each sphere in the initial packing is then allocated to exactly one cell according to the site coordinates of the sphere's center.

B. Rearrangement

The iterative rearrangement algorithm that was developed is shown schematically in Fig. 1. An iteration begins by searching for the nonregistered sphere S_i with the smallest z coordinate; a registered sphere is a stable, overlap-free sphere that is not allowed to move. S_i is then moved a small distance along the vector sum of the overlaps with surrounding spheres ($\mathbf{O}_t$). $\mathbf{O}_t$ is defined as

$$\mathbf{O}_t = \mathbf{O}_x + \mathbf{O}_y + \mathbf{O}_z, \tag{3.4}$$

where

$$\mathbf{O}_x = \mathbf{i}_x \sum_{l=1}^{n_o} \left[(r_i + r_l) - d_{il}\frac{x_i - x_l}{d_{il}} \right], \tag{3.5}$$

$$\mathbf{O}_y = \mathbf{i}_y \sum_{l=1}^{n_o} \left[(r_i + r_l) - d_{il}\frac{y_i - y_l}{d_{il}} \right], \tag{3.6}$$

$$\mathbf{O}_z = \mathbf{i}_z \sum_{l=1}^{n_o} \left[(r_i + r_l) - d_{il}\frac{z_i - z_l}{d_{il}} \right], \tag{3.7}$$

$$d_{il} = \sqrt{(x_i - x_l)^2 + (y_i - y_l)^2 + (z_i - z_l)^2}, \tag{3.8}$$

$\mathbf{i}_x$, $\mathbf{i}_y$, and $\mathbf{i}_z$ are the unit vectors along the x, y, and z directions, respectively, and n_o is the number of spheres overlapping S_i.

Overlaps with stable spheres are searched for, both within the same cell as S_i and in the adjacent 26 cells. Since $d_c = D_m + \delta$, all possible overlaps occur within these 27 cells. The move is accepted as long as the magnitude of $\mathbf{O}_t$ does not exceed the maximum value, $O_{t,m}$. We have found that $O_{t,m} \approx r_o$ maintains an efficient overlap removal process.

The next step is to roll S_i until a stable site is found. Generally, a stable sphere is supported by at least three contacting spheres underneath. More specifically, S_i is stable if the x and y coordinates of its center are within the triangle formed by the x and y coordinates of the centers of any three supporting spheres. A supporting sphere, S_j, is defined as one that contacts S_i and has a site lower than that of S_i, i.e., $z_j < z_i$. For a bridged sphere, a stable condition is achieved when the sphere is not only supported by one or two underlying spheres but also balanced by the lateral support of one or two of its neighbors.

Since smaller spheres are more mobile than larger spheres, they can easily fail to find three supporting spheres; a tendency to move towards the bottom along tortuous paths results—a physically realistic phenomenon. In order to avoid undesired clustering of small particles, however, particles with radii smaller than a certain limit r_c ($r_c = 0.2r_o$) are considered stable when they nest in the saddle formed between two underlying supporting spheres.

When S_i intersects a boundary, an image sphere, S_{im}, is added at the opposite boundary, so as to maintain the periodic boundary condition. If this addition occurs, the program finds the registered spheres overlapping S_i and moves them to the initial packing data.

The process of searching for a stable site for the S_i is repeated until N_s stable sites for S_i are found, where

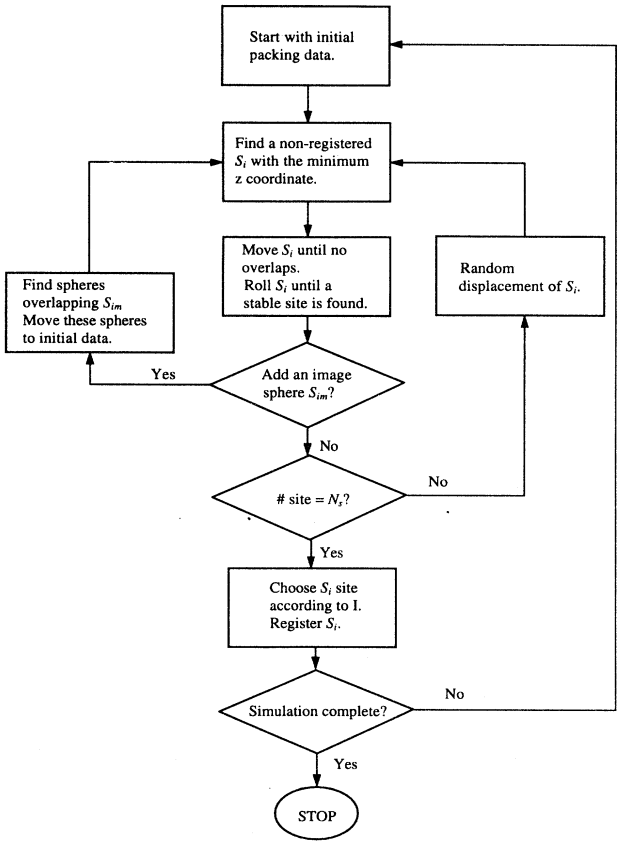

FIG. 1. Main flow chart for sphere rearrangement.

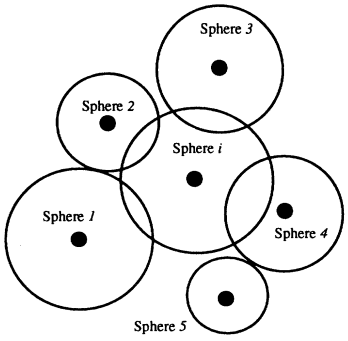

FIG. 2. Special case in which sphere i is locked up in space. Spheres 1, 2, 3, 4, and 5 are registered stable spheres.

N_s is a user-specified parameter. These sites are then indexed such that $z_i(1) > z_i(2) > \cdots > z_i(N_s)$. The final registered site is chosen according to an input control parameter, called the porosity index, I, where $1 \leq I \leq N_s$. The larger I is, the lower the site that is chosen, and therefore the denser the packing that is produced. This iterative process is repeated until the last sphere from the initial packing is registered.

At high initial packing porosities, S_i takes tens of moves to eliminate overlaps. However, as the porosity decreases, the number of moves increases; although moving a sphere along the vector sum of the overlaps reduces some overlaps, it creates or increases others. At low initial packing porosities, some spheres fail to remove overlaps within the allowed N_m steps of movement. When this happens, S_i is given a horizontal displacement by defining

$$x_i^{(1)} = x_i^{(0)} + \delta_1 d_c, \tag{3.9}$$

$$y_i^{(1)} = y_i^{(0)} + \delta_1 d_c, \tag{3.10}$$

where $x_i^{(0)}$ and $y_i^{(0)}$ are previous x and y coordinates for S_i, $x_i^{(1)}$ and $y_i^{(1)}$ are new x and y coordinates for S_i, and $\delta_1 \in [-1, 1]$ is a uniformly distributed random value. Thereafter a new iteration with S_i is started.

At a low initial packing porosity, it is possible for S_i to become locked in a certain space so that it can never get rid of overlaps. A two-dimensional illustration of such a lock up is given in Fig. 2. In this case, the program reduces the size of S_i by 10%, and S_i begins another iteration. Even at low packing porosities, less than 5% of the particles needed to shrink in size. This necessary step in the algorithm resulted in maximum reductions in r_o of less than 0.9% and in σ of less than 0.2%.

IV. RESULTS

A. Random close packing

We have run simulations containing between 10^2 and 5×10^5 spheres; findings showed that both the ϕ and the

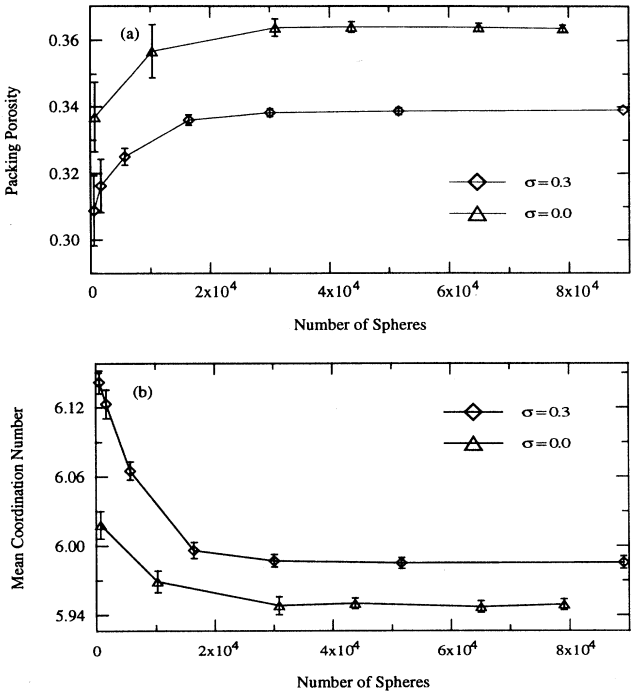

FIG. 3. Random close-packing results as a function of simulation size: (a) packing porosity; (b) mean coordination number.

mean coordination number ($\overline{C_n}$) are variable and thus unreliable if the sample sizes are small. Figure 3 illustrates this effect for both ϕ and $\overline{C_n}$, where the error bars show the standard deviation associated with each data point. Because of the influence of sample size, all the properties presented below are measured for simulations of at least 5×10^4 spheres.

In random close packing (RCP) of uniform spheres, we

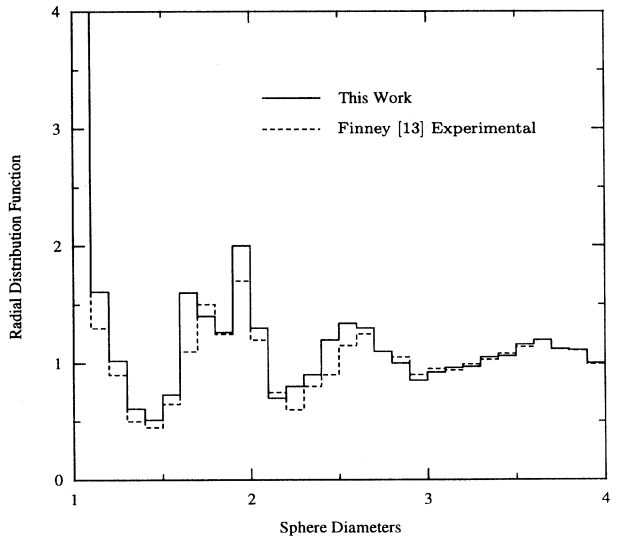

FIG. 4. Simulated versus observed radial distribution function.

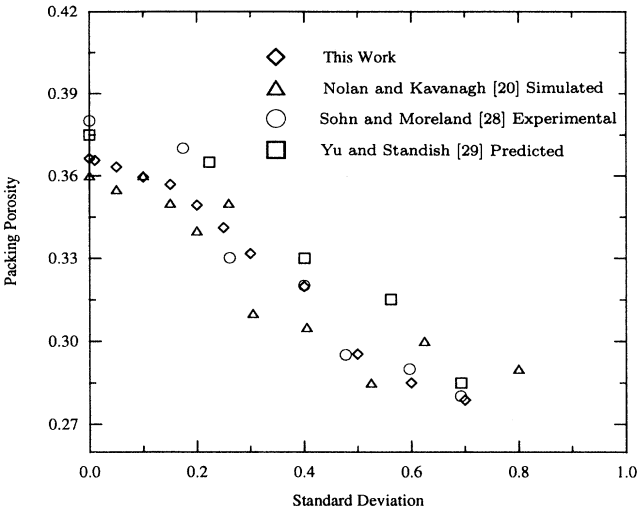

FIG. 5. Packing porosity versus standard deviation for random close packings.

obtained packing porosities from 0.3634 to 0.3635; these values are in excellent agreement with the experimental value of 0.3634 [8,13] and simulated results [18,19]. We observed $\overline{C_n}$ for RCP from 5.94 to 5.95, which is in excellent agreement with the experimental value of ~ 6.0 [24] and simulated results [19,25,26]. The radial distribution function (RDF) for RCP (Fig. 4) exhibits secondary peaks at 1.70, 1.98, 2.65, and 3.60 diam. These features correspond to those of Finney [13] for a ball bearing assembly and to the simulated results using collective rearrangement methods [18,19,27].

The packing porosities from close-packed simulations for different size distributions are plotted as a function of σ in Fig. 5. This figure also shows results of close-packed sands with a spherical coefficient value of 0.86 from the experimental work of Sohn and Moreland [28], simulated packing porosities from Nolan and Kavanagh [20], and theoretical calculations of Yu and Standish [29]. Our results are in excellent agreement with those of Sohn and Moreland and the simulated results of Nolan and Kavanagh, and are close to those of Yu and Standish.

Figure 6 shows the influence of σ on $\overline{C_n}$ for RCP. Results from Powell [26] and Nolan and Kavanagh [20] are shown as well. With an increase in σ, Powell's data remain approximately unchanged, whereas the data of Nolan and Kavanagh show a large increase at $\sigma \approx 0.4$. This increase is probably caused by the small simulation size. It is interesting that $\overline{C_n}$ in our simulation remains stable when the $\sigma < 0.4$, but decreases gradually when $\sigma > 0.4$.

Figure 7 shows the C_n distributions of RCP states for σ of 0.3, 0.5, and 0.7; these distributions are divided into contributions from spheres with different radii. Figure 7(a) shows that at $\sigma = 0.3$, spheres with radii in the range of 0.15–0.25 contribute most to the overall C_n distribution, followed by spheres with radii in the range of 0.25–0.35. For $\sigma = 0.5$, the dominance of spheres with radii in the range of 0.20 and 0.30 decreases, and the contribution from spheres with radii in the range of 0.05–0.15 becomes more important; spheres with radii greater than 0.35 increase their influence on the overall C_n distribution as well [Fig. 7(b)]. These shifts of importance are consistent with the changes of particle size distributions from $\sigma = 0.3$ to $\sigma = 0.5$. These effects become more obvious when $\sigma > 0.7$ [see Fig. 7(c)]. Another interesting finding is that as σ increases from 0.3 to 0.7, $\overline{C_n}$ decreases slightly for spheres with different radii ranges. Generally speaking, then, except for the largest spheres, the number of contacts for each sphere decreases slightly as σ increases.

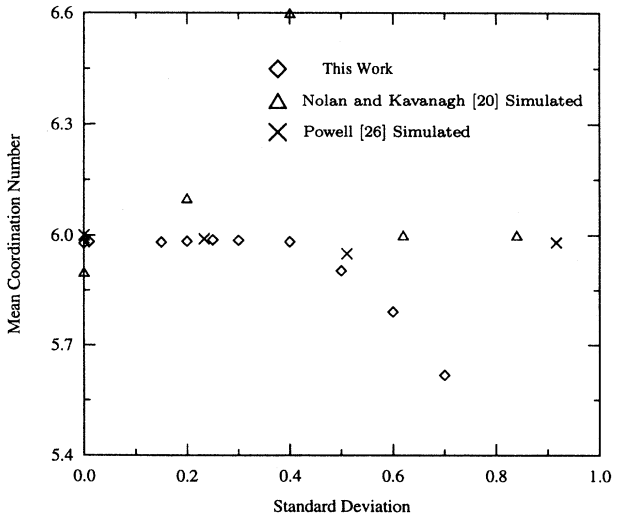

FIG. 6. Mean coordination number versus standard deviation for random close packings.

B. Variable porosity random packing

For this algorithm, ϕ is controlled by ϕ_0, σ, and I. Figure 8 shows ϕ plotted as a function of ϕ_0 and I for a range of σ. Once σ is given, a desired ϕ can be obtained by specifying ϕ_0 and I according to this map. I is chosen such that when $\phi_0 \in (0.45, 0.50]$, $I = 1$; when $\phi_0 \in (0.40, 0.45]$, $I = 2$; etc. The lower ends of the curves correspond to RCP and the upper ends to random loose packing (RLP).

Figure 9 shows ϕ as a function of σ for RLP simulations. An experimental value [30] and simulated results [16,20] are included for comparison. For $\sigma = 0$ (i.e., random packing of uniform spheres) the simulated ϕ is similar to published results. As σ increases, ϕ is consistent with the results from Nolan and Kavanagh [20].

We show $\overline{C_n} = f(\sigma)$ in Fig. 10, along with previously reported results [16,20] for comparison. $\overline{C_n}$ from this research is significantly higher than values of $\overline{C_n}$ found by previous investigators. We believe this discrepancy is due to differences among methods used to simulate particle bridging. In our algorithm, a bridge is formed when a sphere moves and comes in lateral contact with one or

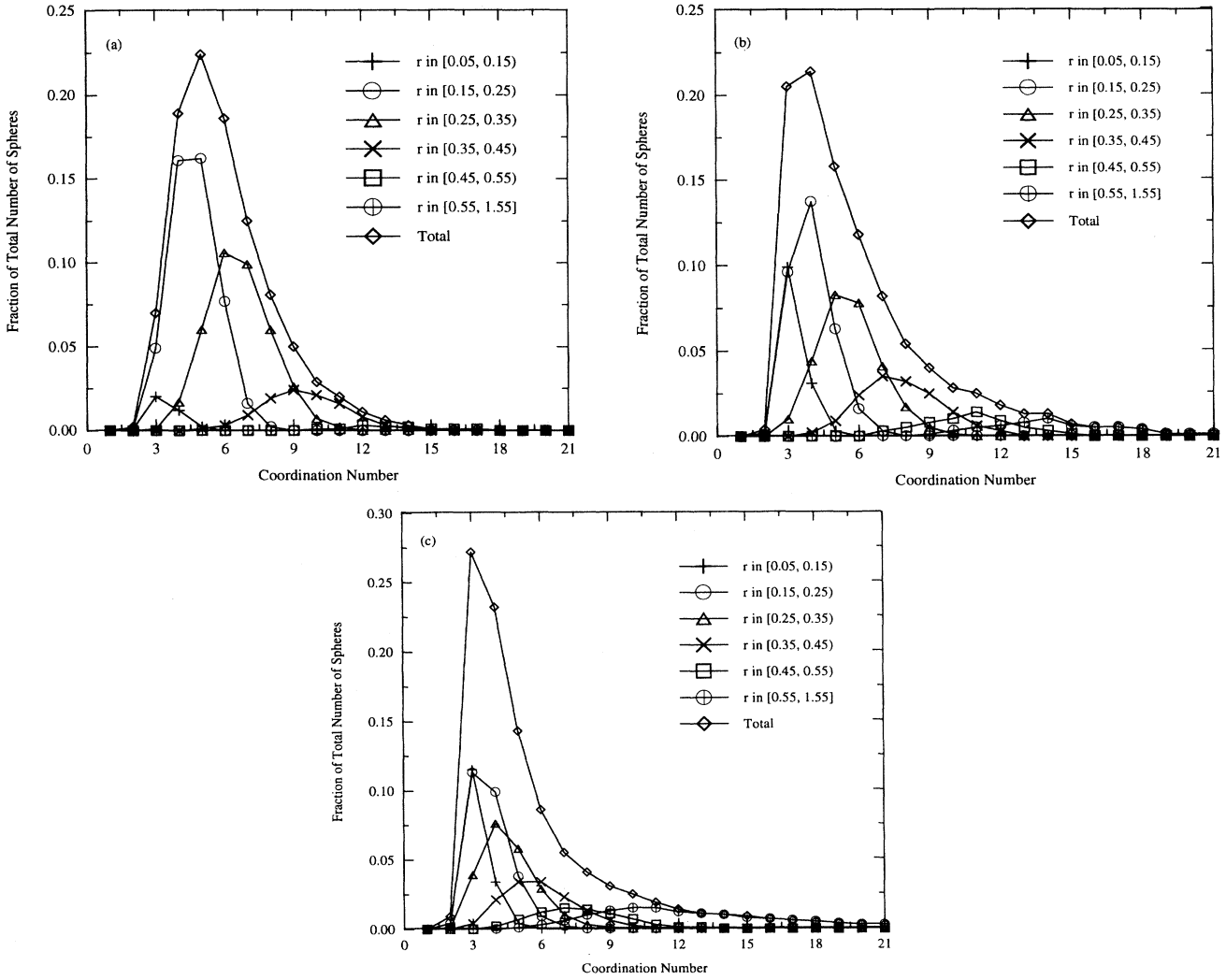

FIG. 7. Distributions of coordination number of RCP states for (a) $\sigma = 0.3$, (b) $\sigma = 0.5$, (c) $\sigma = 0.7$, contributed by spheres of various radius size ranges.

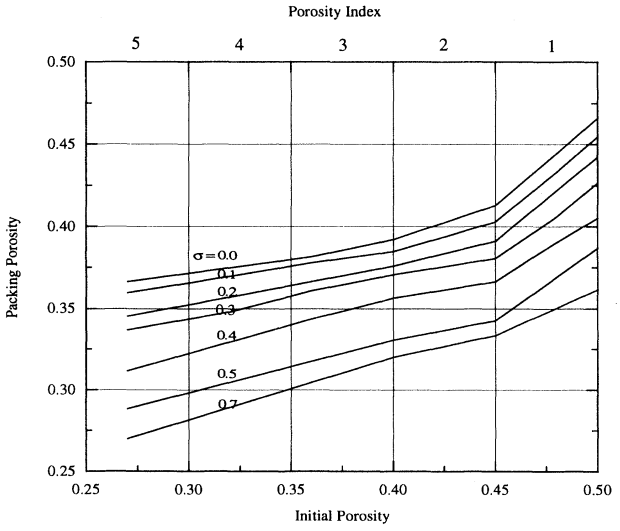

FIG. 8. Packing porosity versus initial porosity and porosity index for various standard deviations.

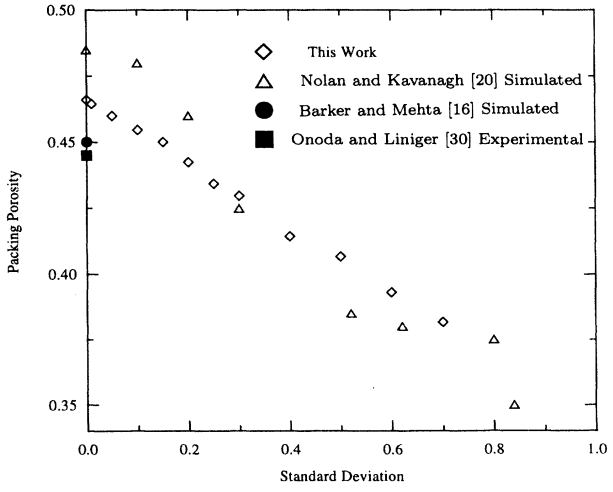

FIG. 9. Packing porosity versus standard deviation for random loose packings.

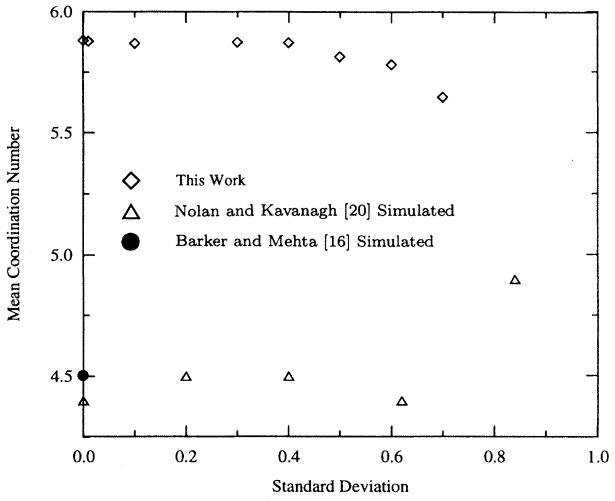

FIG. 10. Mean coordination number versus standard deviation for random loose packings.

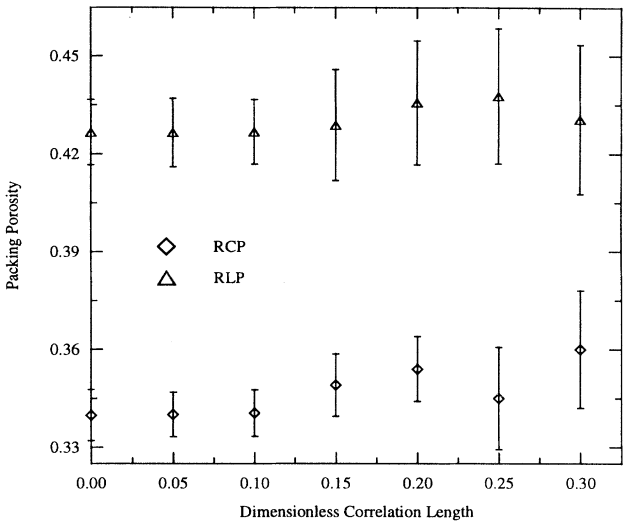

FIG. 12. Effect of correlation length on packing porosity in both the RCP and RLP states.

two stable spheres, whereas in Barker and Mehta's simulation [16], for example, two or more touching spheres are allowed to move simultaneously until a stable configuration is achieved; the production of more bridges is inherent in their approach. Usually, the more bridges that are built, the fewer the contacts with these bridged spheres, causing a lower $\overline{C_n}$ to be obtained. Which of the bridging mechanisms is most realistic is an open research question.

C. Spatially correlated random packing

We have found that both ϕ and $\overline{C_n}$ are strongly influenced by not only the correlation length, l_c, but also σ and the domain size. Figure 11 illustrates this effect for both ϕ and $\overline{C_n}$ in RCP and RLP states, in which the correlation is set such that $l_{cx}/X = l_{cy}/Y \approx 0.1$

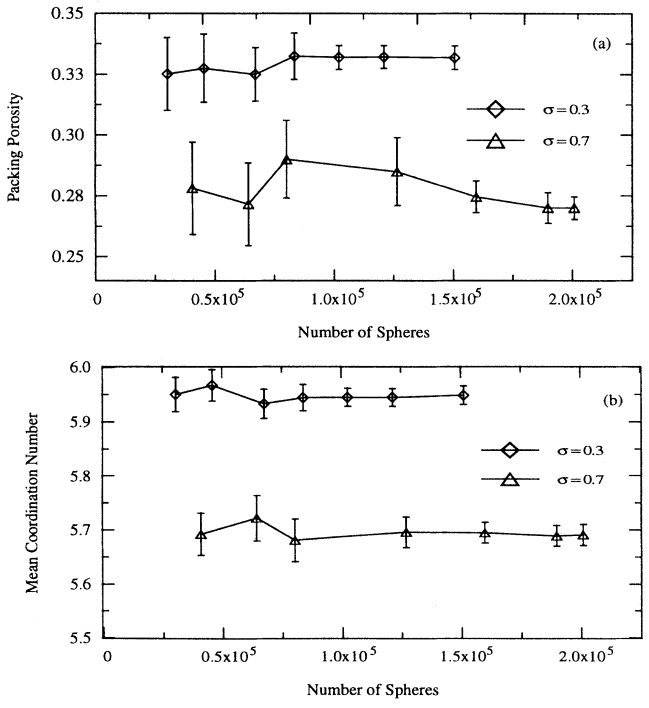

FIG. 11. Random close packing for spatially correlated packing as a function of simulation size and standard deviation: (a) packing porosity, (b) mean coordination number.

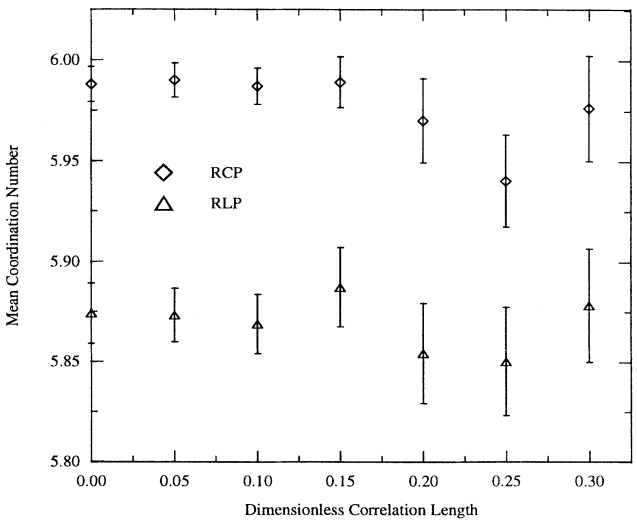

FIG. 13. Effect of correlation length on mean coordination number in both the RCP and RLP states.

and $l_{cz}/Z \approx 0.05$. Error bars represent the standard deviation of each data point. In order to reach a constant state, simulation size increases as a function of increasing σ.

Figures 12 and 13 plot ϕ and $\overline{C_n}$ versus the dimensionless correlation length, L_c, for both the RCP and RLP states, where $L_c = l_{cx}/X = l_{cy}/Y$, $l_{cz}/Z \approx 0.05$. Both ϕ and $\overline{C_n}$ show increasing variation when $l_{cx} > 0.1X$. These simulations were performed with about 5×10^4 spheres. Clearly, much larger simulations would be required to produce results of high precision, especially for large values of L_c.

Figure 14 shows different layers of the packing with $\sigma = 0.3$, $r_o = 0.25$, $l_{cx} = l_{cy} \approx 3.5 \times D_m$, and $l_{cz} \approx D_m$. Each image is created at a height of two D_m above the previous layer. The effect of the correlation structure can clearly be seen on these images. Such spatial correlation is typical of natural systems [6], and we know of no other simulator that includes this feature. Future work will focus on quantifying correlation structures using advanced

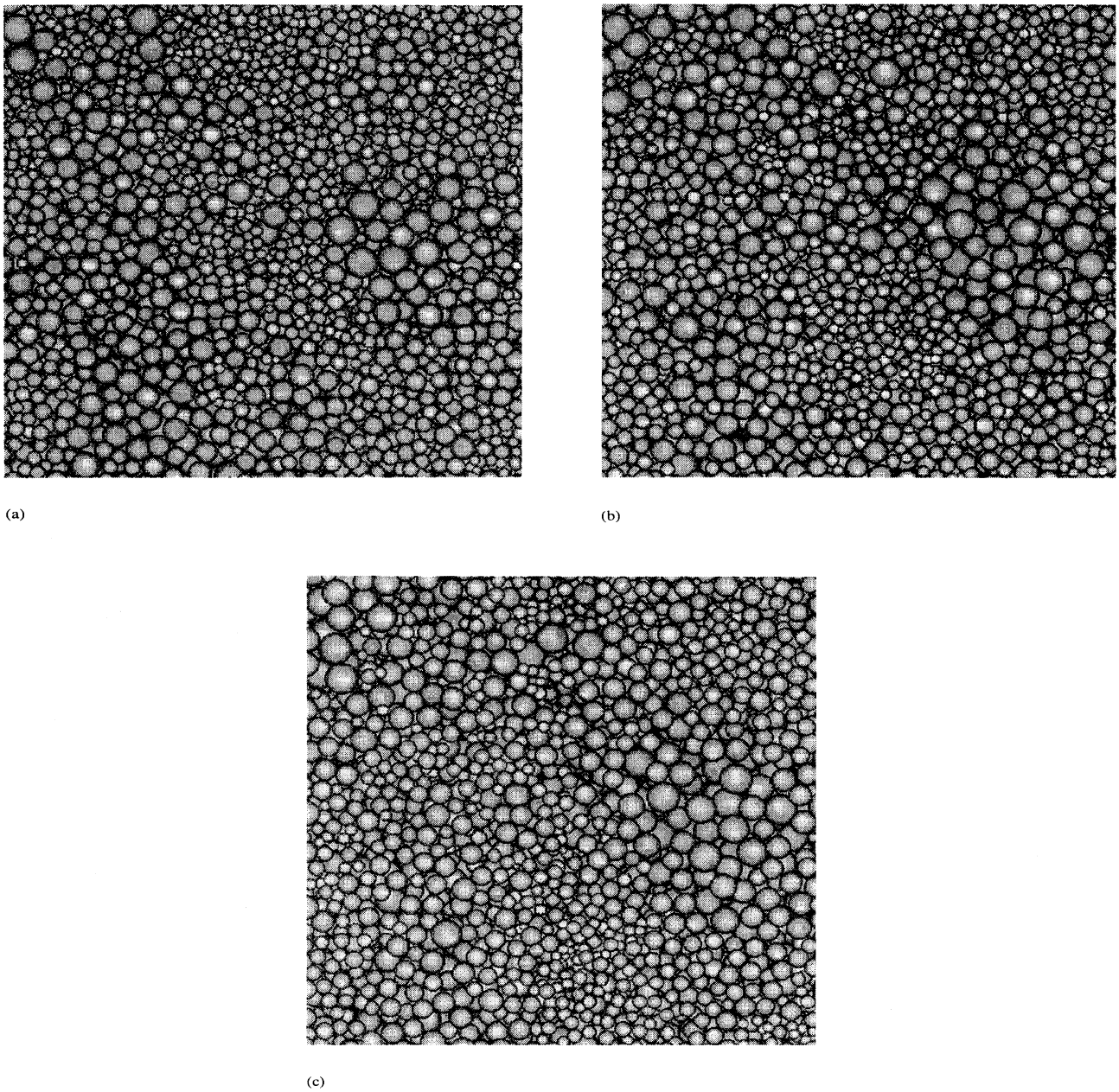

(a) (b) (c)

FIG. 14. Visualization of a spatially correlated random packing, where each image has an approximate size of $5l_c$.

imaging techniques and solving for transport phenomena at the pore scale in such systems.

V. CONCLUSIONS

An algorithm to simulate gravitationally stable random packings of spheres with log-normal particle size distributions was developed and applied. Evaluation of the packing porosity, coordination number distribution, and radial distribution leads to the following conclusions:

1. The packing porosity for both random close packing and random loose packing consistently decreases as the standard deviation of the particle size increases.
2. Both the packing porosity and mean coordination number attain near-constant states when the number of packed spheres is greater than 3×10^4 for a purely random packing.
3. The mean coordination number decreases as the standard deviation of the particle size distribution increases to values greater than 0.5 for both random close packing and random loose packing states.
4. For correlated random packing conditions, the size of the simulation required to achieve a given standard deviation of either the mean porosity or the mean coordination number depends upon the correlation length of the covariance function and the standard deviation of the particle size distribution. For a given correlation length, the higher the standard deviation, the larger the domain size that is required to minimize variations of packing porosity and the mean coordination number.

ACKNOWLEDGMENTS

This work was supported by Grant No. DAAL03-92-G-0111 from the Army Research Office.

[1] W. G. Gray, A. Leijnse, R. L. Kolar, and C. A. Blain, *Mathematical Tools for Changing Scales in the Analysis of Physical Systems* (CRC Press, Inc., Boca Raton, 1993).
[2] J. Bear, *Dynamics of Fluids in Porous Media* (Dover Publications, Inc., New York, 1972).
[3] G. de Marsily, *Quantitative Hydrogeology: Groundwater Hydrology for Engineers* (Academic Press, Orlando, FL, 1986).
[4] J. Bear and Y. Bachmat, *Introduction to Modeling of Transport Phenomena in Porous Media* (Kluwer Academic Publishers, Dordrecht, The Netherlands, 1991).
[5] N. S. Martys, S. Torquato, and D. Bentz, Phys. Rev. E **50**, 403 (1994).
[6] G. Christakos, *Random Field Models in Earth Sciences* (Academic, New York, 1992).
[7] A. S. Mayer and C. T. Miller, J. Contaminant Hydrology **11**, 189 (1992).
[8] C. H. Bennett, J. Appl. Phys. **43**, 2727 (1972).
[9] W. M. Visscher and M. Bolsterli, Nature **239**, 504 (1972).
[10] J. F. Sadoc, J. Dixmier, and A. Guinier, J. Non.-Cryst. Solids **12**, 61 (1973).
[11] A. J. Matheson, J. Phys. C **7**, 2569 (1974).
[12] R. Jullien and P. Meakin, Europhys. Lett. **4**, 1385 (1987).
[13] J. L. Finney, Mater. Sci. Eng. **23**, 199 (1976).
[14] J. G. Berryman, Phys. Rev. A **27**, 1053 (1983).
[15] J. P. Hansen and I. R. McDonald, *Theory of Simple Liquids* (Academic Press, Harcourt Brace Jovanovich, London, 1986).
[16] G. C. Barker and A. Mehta, Phys. Rev. A **45**, 3435 (1992).
[17] W. F. van Gunsteren, Mol. Simul. **3**, 187 (1989).
[18] A. S. Clarke and J. Wiley, Phys. Rev. B **35**, 7350 (1987).
[19] G. T. Nolan and P. E. Kavanagh, Powder Technol. **72**, 149 (1992).
[20] G. T. Nolan and P. E. Kavanagh, Powder Technol. **76**, 309 (1993).
[21] W. A. Gray, *The Packing of Solid Particles* (Chapman and Hall, London, 1968).
[22] G. Herdan, *Small Particle Statistics* (Buttterworths, London, 1960).
[23] C. V. Deutsch and A. G. Journel, *GSLIB: Geostatistical Software Library and User's Guide* (Oxford University Press, New York and Oxford, 1992).
[24] J. D. Bernal, Nature **185**, 68 (1960).
[25] W. S. Jodrey and E. M. Tory, Phys. Rev. A **32**, 2347 (1985).
[26] M. J. Powell, Powder Technol. **25**, 45 (1980).
[27] W. S. Jodrey and E. M. Tory, Powder Technol. **30**, 111 (1981).
[28] H. Y. Sohn and C. Moreland, Canadian J. Chem. Eng. **46**, 162 (1968).
[29] A. B. Yu and N. Standish, Powder Technol. **55**, 171 (1988).
[30] G. Y. Onoda and E. Liniger, Phys. Rev. Lett. **64**, 2727 (1990).

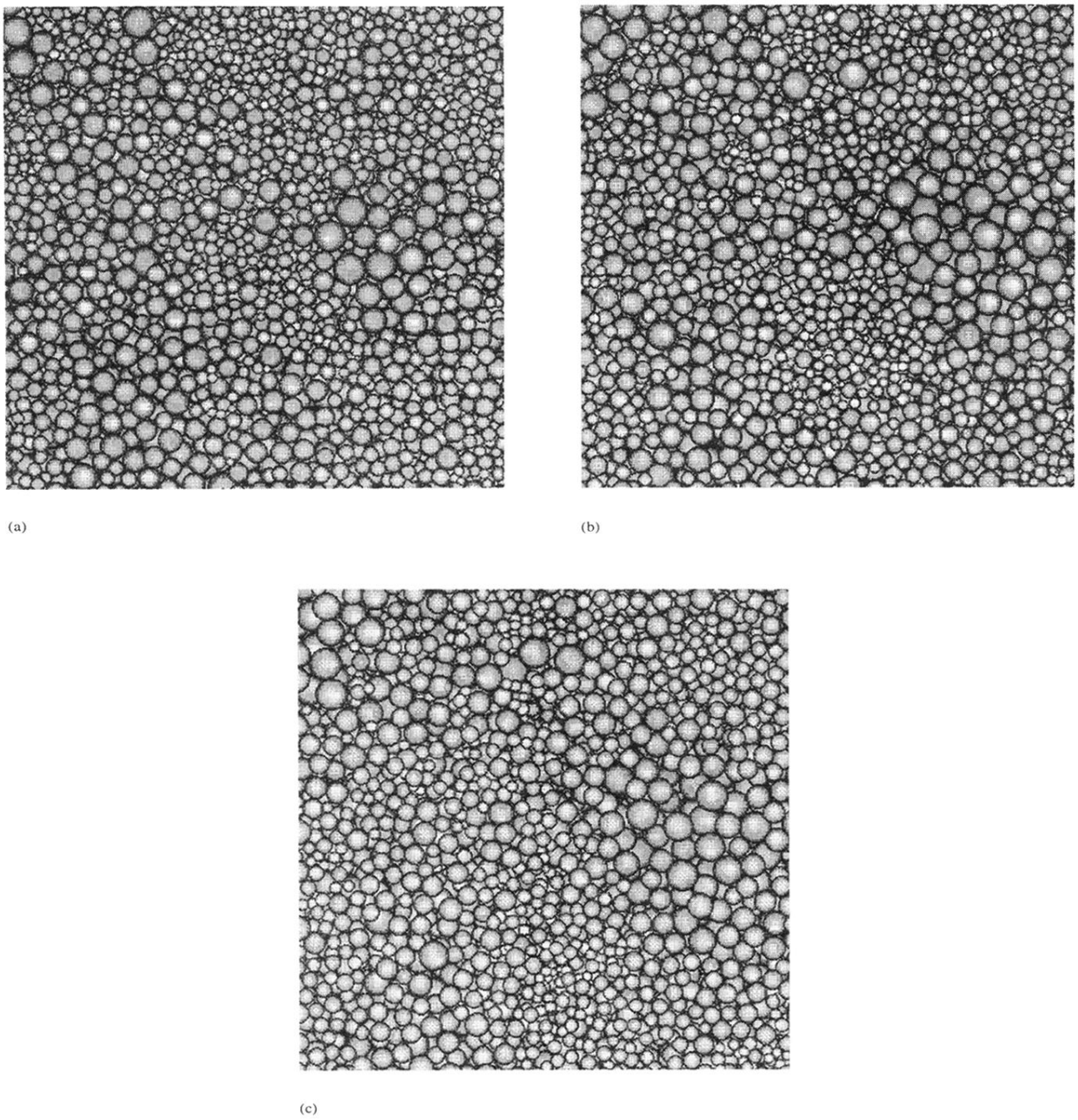

(a)

(b)

(c)

FIG. 14. Visualization of a spatially correlated random packing, where each image has an approximate size of $5l_c$.